Nanoelectrochemistry of mammalian cells

Peng Sun, François O. Laforge, Thushara P. Abeyweera, Susan A. Rotenberg, James Carpino, and Michael V. Mirkin*

Department of Chemistry and Biochemistry, Queens College–City University of New York, Flushing, NY 11367

Communicated by Allen J. Bard, University of Texas, Austin, TX, November 21, 2007 (received for review October 2, 2007)

There is a significant current interest in development of new techniques for direct characterization of the intracellular redox state and high-resolution imaging of living cells. We used nanometer-sized amperometric probes in combination with the scanning electrochemical microscope (SECM) to carry out spatially resolved electrochemical experiments in cultured human breast cells. With the tip radius ≈1,000 times smaller than that of a cell, an electrochemical probe can penetrate a cell and travel inside it without apparent damage to the membrane. The data demonstrate the possibility of measuring the rate of transmembrane charge transport and membrane potential and probing redox properties at the subcellular level. The same experimental setup was used for nanoscale electrochemical imaging of the cell surface.

charge transfer | membrane potential | scanning electrochemical microscopy | voltammetry

The changes in intracellular redox state can be related to various pathological conditions such as oxidative stress (1), diabetes (2), and cancer (3). Electrochemical measurements can provide comprehensive information about intracellular redox states, including concentrations of redox species, kinetics of redox reactions, and charge transport rates. Microelectrodes positioned near the cell surface (4, 5) and the scanning electrochemical microscope (SECM) (6–8) have been used for such measurements. The applications ranged from dopamine (4) and cholesterol (9) analysis to studies of menadione metabolism in yeast (10) and hepatoblastoma cells (11) to detection of reactive oxygen species (12) and monitoring the drug efflux from cancer cells (13). The SECM was also used for micrometer-scale topographic and reaction rate imaging of various types of biological cells (14–17).

We have shown that intracellular redox activity can be probed noninvasively by measuring the rate of transmembrane charge transfer (CT) by using the feedback mode of the SECM operation (17). In such experiments, the tip electrode is placed in solution containing the oxidized (or reduced) form of a redox mediator. A mediator species is then reduced (or oxidized) at the tip electrode. A piezo-positioner is used to move the tip toward the surface of an immobilized cell. If the mediator species is hydrophobic, the product of the tip reaction can cross the cell membrane and be reoxidized (or rereduced) by intracellular redox reaction (Fig. 1*A*). This process can produce an enhancement in the faradaic current at the tip electrode (positive feedback) depending on the mediator regeneration rate and the tip/membrane separation distance (d). If the mediator is hydrophilic, it cannot cross the cell membrane, which blocks the diffusion of species O to the tip (Fig. 1*B*), so the tip current (i_T) decreases with d (negative feedback). Some useful information about intracellular redox state was extracted from the analysis of i_T vs. d curves (17). However, the mechanism of mediator regeneration by the cell is rather complicated, and the need to include transmembrane CT processes makes the data analysis even more difficult (18).

More informative and easier to interpret data could be obtained by making electrochemical measurements inside an immobilized cell or by using "artificial cells" (19, 20). Only a few examples of intracellular electrochemical measurements have been reported to date (21–23). One of the main obstacles here is the electrode size and geometry; even a sharp, conical electrode puncturing a lipid membrane may cause a solution leakage (20). Also, one would need nanometer-sized electrodes for spatially resolved intracellular measurements, and the characterization of conical nanoelectrode geometry is challenging (24).

Here, we report the use of the SECM equipped with well characterized polished nanotips (radius, $a \geq 10$ nm) for spatially resolved quantitative experiments inside living cells (Fig. 1*C*). In this way, one can determine the mass/charge transfer rate across the cell membrane (Fig. 1*D*), evaluate the membrane potential, and measure the redox properties with a nanoscale resolution. Very sharp tips (Fig. 1*E*) with the radius of insulating glass, $r_g \cong 3a$ were used to minimize the mechanical damage to the cell.

Because the thickness of the diffusion layer is equal to a few nanoelectrode radii, a nanoprobe "sees" only local electrochemical properties of a nanometer- or a submicrometer-sized domain. In a system as complicated as a living cell, the ability to probe the local redox environment instead of analyzing complicated response originating from different subcellular compartments is an important advantage. The high spatial resolution offered by nanotips can also be used for nanoscale imaging of cellular topography and surface reactivity that could be complementary to atomic force microscopy (AFM) (25), scanning ion-conductance microscopy (26), and "superresolution" optical methods (27).

Results

SECM Measurements and Intracellular Voltammetry. The current vs. distance ($i_T - d$) curve in Fig. 2*A* was obtained with a hydrophilic redox mediator, 1 mM $Ru(NH_3)_6^{3+}$, which could not permeate the cell membrane acting as an insulator. A 42-nm polished Pt tip approached and penetrated an immobilized MCF-10A cell (positive d corresponds to the tip approaching the membrane; negative distances—within the cell volume). The experimental approach curve (symbols) fits the SECM theory (28) (solid line) for $d \geq 0.5a$ at which the tip began to push the cell membrane. One should notice that the tip/membrane separation distance at the point of the closest approach is ≈20 nm. This indicates that the SECM equipped with a nanometer-sized tip can potentially be used for topographic imaging of cell surfaces with a ≈20-nm scale resolution.

At $d \cong -1.2a$, the tip gets inside the cell, and the current vanishes. Accordingly, the wave of $Ru(NH_3)_6^{3+}$ reduction was observed in the outer buffer solution (Fig. 2*B*, curve 1) but not inside the cell (curve 2). This indicates that the membrane immediately forms a tight seal around the penetrating nanotip that prevents the external solution from leaking inside the cell. The use of a small and very sharp tip (Fig. 1*E*) is essential here: the maximum radius of the electrode portion inserted into the cell is $\ll 1$ μm even when the length of that part is ≈5 μm. (One should notice that the tip of the nanoelectrode is not visible in Fig. 1*E*.)

Author contributions: M.V.M. designed research; P.S. and F.O.L. performed research; F.O.L., T.P.A., S.A.R., and J.C. contributed new reagents/analytic tools; M.V.M. analyzed data; and P.S. and M.V.M. wrote the paper.

The authors declare no conflict of interest.

*To whom correspondence should be addressed. E-mail: mmirkin@qc.cuny.edu.

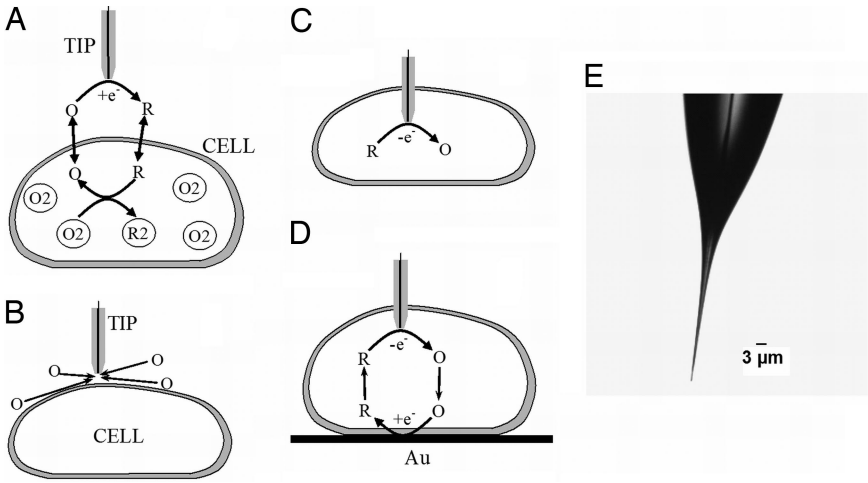

Fig. 1. Schematic diagrams of the SECM experiments with single cells (*A–D*) and an optical micrograph of a typical nanotip used in such experiments (*E*). (*A*) The tip is positioned in the solution close to the cell surface. Positive feedback is due to bimolecular electron transfer between hydrophobic redox mediator (O/R) and cell-bound redox moieties (O2/R2). (*B*) The lipid cell membrane is impermeable for a hydrophilic redox mediator. Negative feedback is due to the hindered diffusion of redox species to the tip electrode. (*C*) Nanoelectrode voltammetry inside the cell. (*D*) Positive feedback is produced by mediator regeneration by way of electron transfer at the underlying Au surface.

In contrast to $Ru(NH_3)_6^{3+}$, the oxygen reduction wave inside the cell (Fig. 2*B Inset*, pink curve) is very similar to that measured outside (Fig. 2*B Inset*, blue curve at $E \lesssim -400$ mV) because of rapid oxygen transport across the membrane. This wave disappeared when the solution was purged with nitrogen to remove O_2 (Fig. 2*B*, curve 2). From curve 2, one also can see that the concentration of mobile redox species in the cell is very low. Our previous experiments (17, 18) showed that the effective

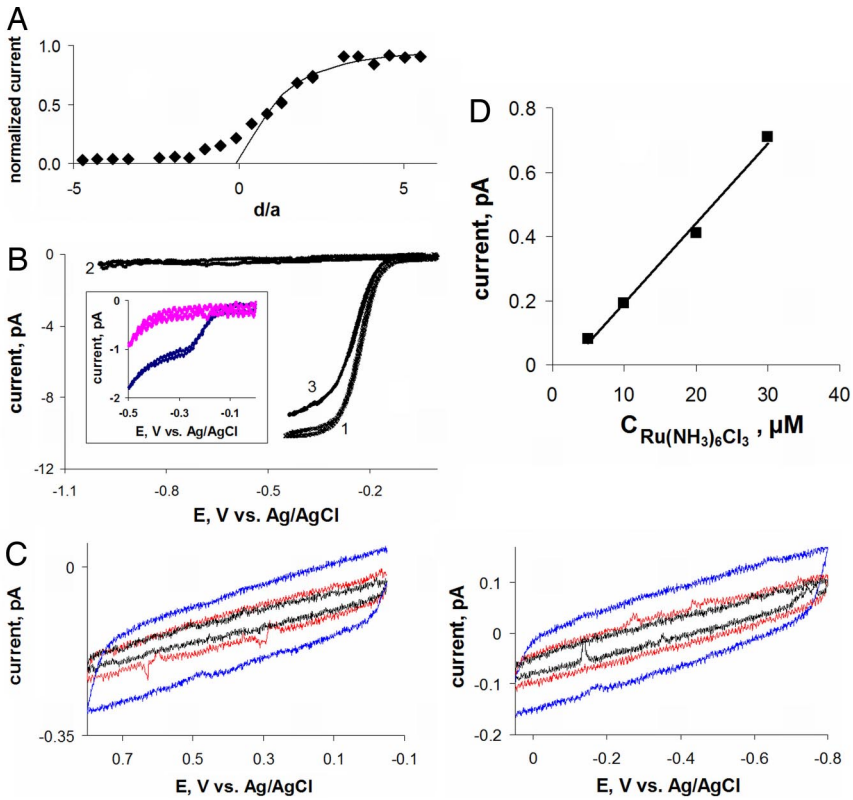

Fig. 2. Current vs. distance curve obtained with a Pt tip approaching and penetrating an MCF-10A cell (*A*) and voltammograms obtained at nanoelectrodes inside living cells and in solution (*B–D*). (*A*) Solid line is the theoretical curve for an insulating substrate (28). The tip current is normalized by the value measured in the bulk solution. The approach speed was 20 nm/s. (*B*) Voltammograms obtained in the bulk solution outside of the cell (curve 1), inside the cell (curve 2), and in external solution after the tip was withdrawn from the cell (curve 3). (*Inset*) Voltammograms obtained in PBS (blue) and inside the cell (pink) without purging the solution with nitrogen. (*C*) Intracellular voltammograms obtained by scanning the electrode potential between 0 and +0.8 V (*Left*) and 0 and −0.8 V (*Right*). The scan rate was (in mV/s): 50 (blue), 20 (red), and 10 (black). The concentration of $Ru(NH_3)_6Cl_3$ in PBS was 1 mM (*A–C*) and 0.1 mM (*B Inset*). (*D*) Dependence of the steady-state diffusion limiting current vs. concentration of $Ru(NH_3)_6Cl_3$. The tip radius (in nm) was: 42 (*A*), 39 (*B*), 54 (*C*), and 73 (*D*).

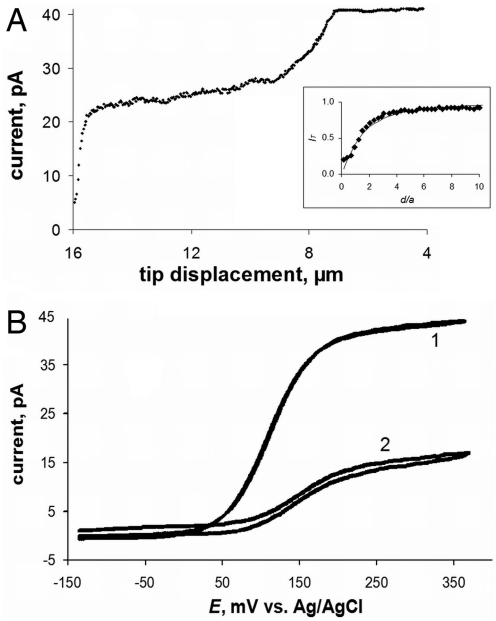

Fig. 3. Approach and penetration of an MCF-10A cell by a 144-nm tip in PBS solution containing 1 mM $FcCH_2OH$ (*A*) and steady-state voltammograms obtained at the same tip outside (curve 1) and inside (curve 2) the cell (*B*). (*A Inset*) Shown is the fit between the experiment (symbols) and the theory (solid line) for the final part of the curve, where the tip approaches the bottom of the Petri dish.

concentration of redox centers in the cell, which can be reduced (or oxidized) within the potential window in Fig. 2*B*, is ≥1 mM. Thus, most (if not all) of those redox moieties are immobilized and cannot freely diffuse in the cytoplasm. We used a home-built ultrasensitive potentiostat to check whether micromolar concentrations of any mobile redox species can be detected inside the cell. The voltammograms in Fig. 2*C* were obtained by scanning the tip potential in either positive (*Left*) or negative (*Right*) direction. No voltammetric waves were detected in the curves obtained at different scan rates. The sensitivity of these measurements can be evaluated from Fig. 2*D*, which presents a calibration curve for a 73-nm tip obtained with a concentration of $Ru(NH_3)_6^{3+}$ ranging from 5 to 50 μM. Clearly, the oxidation-reduction of ≤1 μM species should be detectable in our experiments.

The approach curves and intracellular voltammograms in Fig. 3 obtained with a hydrophobic mediator, ferrocenemethanol ($FcCH_2OH$) that can cross the lipid membrane are very different. In this case, i_T decreased and then stabilized at a nonzero value after the tip penetrated the cell (Fig. 3*A*). The well shaped voltammograms of $FcCH_2OH$ were obtained both in the outer solution (Fig. 3*B*, curve 1) and inside the cell (curve 2). Four distinct regions can be seen in the approach curve in Fig. 3*A*. The essentially flat initial part (tip displacement, $l \lesssim 7$ μm) corresponds to the tip/cell distances much longer than a. Negative feedback is observed when the tip moves closer to the cell, pushes the membrane, and finally penetrates it at $l \cong 9$ μm. Because $FcCH_2OH$ is present inside the cell, the exact penetration moment is harder to detect than in the case of a hydrophilic redox mediator (Fig. 2*A*). When the tip is inside the cell but close to the membrane, the measured current is ≈30–40% lower than that in the outer solution. This difference can be attributed to the lower diffusion coefficient of $FcCH_2OH$, and it is consistent with the relative viscosity (cytoplasm vs. water) of 1.5 (29). A slight decrease in the tip current occurring in the next part of the approach curve (9 μm ≲ l ≲ 14.5 μm) corresponds to the concentration profile of $FcCH_2OH$ inside the cell.

A much steeper current decay in Fig. 3*A* occurs when the tip approaches the bottom of the cell that is attached to the insulating plastic surface (15 μm ≲ l). An excellent fit between the experimental data and theory in Fig. 3*A* (*Inset*) suggests the possibility of spatially resolved, quantitative intracellular measurements. This result is in accordance with the high quality of voltammograms of hydrophobic mediators obtained inside the cell (e.g., Fig. 3*B*, curve 2). A number of reproducible intracellular voltammograms were recorded during a period of several minutes. Furthermore, the voltammograms of $Ru(NH_3)_6^{3+}$ and $FcCH_2OH$ measured after withdrawing the tip from the cell were similar to those obtained before the cell penetration (Fig. 2*B*, curves 1 and 3). A usual concern in bioelectrochemistry is that the electrode response may be affected by protein adsorption and fouling of its surface. Apparently, surface fouling was not an issue in our nanoelectrode experiments.

Cell viability was verified by trypan blue exclusion experiments. Because live cells pump out this dye, but dead cells do not, dead cells appear blue, but live cells appear uncolored. After the tip was withdrawn from the cell (which was not possible in a few cases when the cell adhesion to the dish surface was not sufficiently strong), ≈5 μM solution of trypan blue was added to the cell medium. In this way, MCF-10A cells were confirmed to be viable 1–2 h after intracellular electrochemical experiments.

Evaluation of the Membrane Potential. The tip potential in both curves in Fig. 3*B* was measured with respect to the same Ag/AgCl reference electrode located in PBS outside the cell. The 36-mV difference between the half-wave potentials ($\Delta E_{1/2}$) in curves 2 and 1 can be attributed to the potential drop across the cell membrane. This experiment was repeated with 18 different MCF-10A cells and different nanoelectrodes (19 nm ≤ a ≤ 182 nm) yielding $\Delta E_{1/2} = 46 \pm 4$ mV (the uncertainty is expressed as a 95% confidence interval). $\Delta E_{1/2}$ was also measured for three MCF-10A cells bathed in PBS that contained a different hydrophobic redox species (TMPD). Although the quality of intracellular voltammograms of TMPD was not as high as for $FcCH_2OH$, a similar mean value, $\Delta E_{1/2} = 39$ mV, was obtained for this system.

$\Delta E_{1/2}$ was also measured after 600 nM valinomycin was added to PBS without removing the tip from the cell. Valinomycin, which depolarizes the membrane by acting as a potassium carrier, was expected to diminish the membrane potential. In each of these experiments, which were done for seven MCF-10A cells, the $\Delta E_{1/2}$ decreased markedly, and the mean value was 16.7 mV for $FcCH_2OH$ mediator.

Although there is some variability in the membrane potential values reported in the literature, our $\Delta E_{1/2}$ values are somewhat more positive than most numbers obtained for mammalian cells by different techniques (e.g., −58.6 mV to −2.7 mV reported for MCF-7 human mammary tumor cells in ref. 30). To determine whether this difference results from membrane polarization that may be induced by current flowing between the intracellular nanoprobe and the external reference electrode, we measured the dependence of $\Delta E_{1/2}$ on concentration (c_{FcCH_2OH}). The ohmic potential drop across the membrane (iR, where R is the membrane resistance) is proportional to current flowing at the tip electrode inserted in the cell. Five voltammograms in Fig. 4*A* were obtained with the same 112-nm tip in the bulk solution (curve 1) and inside the same cell (curves 2–5). By changing c_{FcCH_2OH} in solution, we measured the linear concentration dependence of the tip current corresponding to the half-wave potential [$i(E_{1/2})$; Fig. 4*B*]. The $\Delta E_{1/2}$ value decreased on dilution of $FcCH_2OH$, and the $\Delta E_{1/2}$ vs. $i(E_{1/2})$ plot was also linear (Fig. 4*C*). The membrane resistance extracted from the slope of this line is ≈4 GΩ. The extrapolation of the $\Delta E_{1/2}$ vs. $i(E_{1/2})$

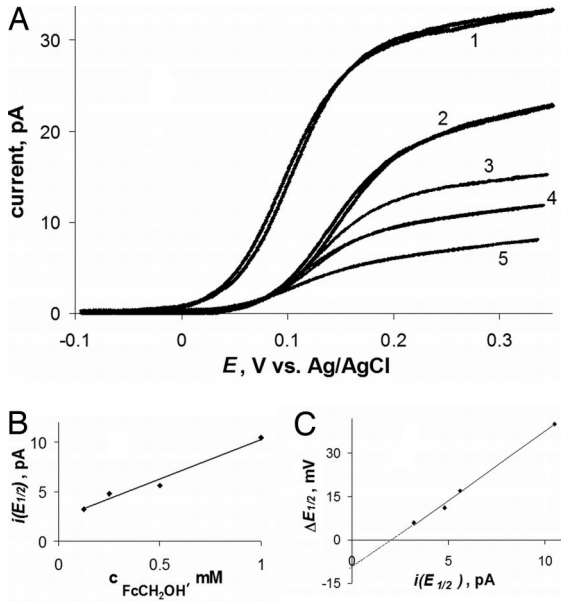

Fig. 4. Voltammograms of $FcCH_2OH$ at a 112-nm Pt tip obtained in the bulk solution (curve 1) and inside the same cell (curves 2–5) (*A*), and corresponding dependences of $i(E_{1/2})$ vs. c_{FcCH_2OH} (*B*) and $\Delta E_{1/2}$ vs. $i(E_{1/2})$ (*C*). (*A*) c_{FcCH_2OH} (in mM) was: 1 (curves 1 and 2), 0.5 (curve 3), 0.25 (curve 4), and 0.125 (curve 5).

dependence to zero current shows that the membrane potential corrected for the polarization effect is somewhat more negative (e.g., ≈ -10 mV in Fig. 4*C*).

Measuring the Mass/Charge Transfer Rate Across the Cell Membrane. In these experiments, the cells were immobilized on a conductive surface, that is, a glass slide coated with an evaporated Au film. Menadione, which can readily cross the MCF-10A cell membrane (17), was used as a redox mediator. Its reduced form (menadiol) was generated at the tip and reoxidized at the Au surface (Fig. 1*D*). SECM approach curves (Fig. 5) were obtained by moving the tip downward inside the cell until its insulator sheath began to push against the membrane and the underlying surface. Because the mediator regeneration at the Au surface is rapid, it was possible to evaluate the mass transfer rate of mediator species across the membrane from the tip current vs. distance curve. When the feedback current is controlled by the rate of membrane transport, the shape of i_T vs. d curve can be described by an equation derived for the finite heterogeneous kinetics of the mediator regeneration at the substrate (18). Fitting an experimental current vs. distance curve to the theory

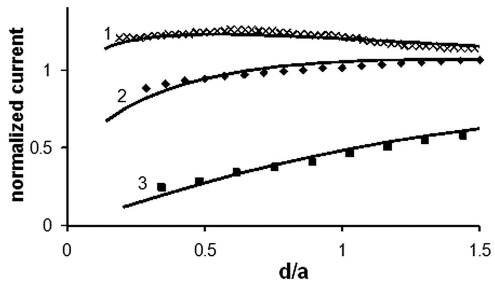

Fig. 5. Evaluating the rate of charge/mass transport across the cell membrane from SECM approach curves. The tip radius (in nm) was: 790 (curve 1), 280 (curve 2), and 146 (curve 3). Experimental data (symbols) was fitted to the theory (solid lines) for finite charge transport kinetics (31) (curves 1 and 2) and pure negative feedback (28) (curve 3).

(31) yields the dimensionless heterogeneous rate constant, $\kappa = Pa/2D$, where $P = KD_m/l_m$ is the permeability coefficient; D and D_m are the diffusion coefficients of redox species in the cytoplasm and in the membrane, respectively; K is the solution-to-membrane partition coefficient of the redox species; and l_m is the membrane thickness.

Curves 1 and 2 in Fig. 5 were obtained with 790-nm and 280-nm tips and yielded the κ values of 1.01 and 0.42, respectively. The difference between the corresponding P values (with $D = 4.7 \times 10^{-6}$ cm^2/s, the menadione diffusion coefficient in cytoplasm), that is, 0.13 cm/s and 0.15 cm/s, is within the range of our experimental error. Curve 3 in Fig. 5 was obtained with a smaller, 146-nm tip, for which the expected κ was $\approx$0.2. This value is close to the lower limit for the rate constant measurable by SECM. Therefore, curve 3 could be fit to the SECM theory for an insulating substrate, and no reliable P value could be extracted from it.

Nanoscale Electrochemical Imaging of Cell Membranes. Two SECM images of MCF-10A cells are shown in Fig. 6. A 11.8 μm $\times$ 11.2 μm constant-current image (Fig. 6*A*), representing most of the cell surface, was obtained with a 123-nm tip in PBS containing 1 mM $Ru(NH_3)_6^{3+}$. Although some topographic features visible in the SECM image can also be found in the optical micrograph of the same cell (Fig. 6*B*), no close similarity can be expected because Fig. 6*B* is a transmitted light picture obtained by using the inverted microscope. The spatial resolution of the SECM image is $\approx$200 nm.

Because the spatial resolution of SECM is determined by the tip radius (31), one can "zoom in" on a small area of the cell membrane by using a smaller tip. In Fig. 6*C*, a 0.6 μm $\times$ 1.5 μm area was imaged in a constant-height mode by using a 47-nm probe. The tip was moved vertically toward the cell, and the resulting current vs. distance curve (similar to that in Fig. 2; data not shown) was recorded. The approach was stopped before the tip current deviated from the theory, that is, before the insulating sheath began to push the membrane. To obtain the image, the tip was scanned laterally in the *x-y* plane above the cell. The lateral resolution of such an image is better than 100 nm, and it can be further improved by decreasing the tip/membrane separation distance.

Discussion

Quantitative electrochemical measurements inside a living cell can be done to evaluate potentials, concentration profiles, and charge transfer kinetics. The very small size of the used nanoprobes allows one to minimize the damage to the cell and to achieve high spatial resolution. However, intracellular redox moieties are apparently localized and cannot diffuse freely within the cell (Fig. 2 *B* and *C*). This necessitates the use of a redox mediator in intracellular voltammetry. To probe enzymatic redox reactions, the mediator concentration must be on the micromolar scale (18), and very low (fA-range) currents have to be measured. Another difficult problem is to precisely position a nanoelectrode at a specific location within the cell (e.g., in proximity to a mitochondrion). In the future, it may be possible to address this issue by using redox-sensitive fluorescent labels.

Previously developed approaches to evaluation of the membrane potential [e.g., those based on cell-attached patches (32), ion-selective probes (33), and fluorescent dyes (34)] have numerous shortcomings from the relatively large size of a potentiometric probe to ambiguity of data analysis (32). Intracellular voltammetry is a relatively straightforward method, in which the membrane potential is evaluated with no additional assumptions or complicated data analysis. The measurements should be made with the mediator concentration as low as feasible to minimize the ohmic potential drop across the membrane. $\Delta E_{1/2}$ varies

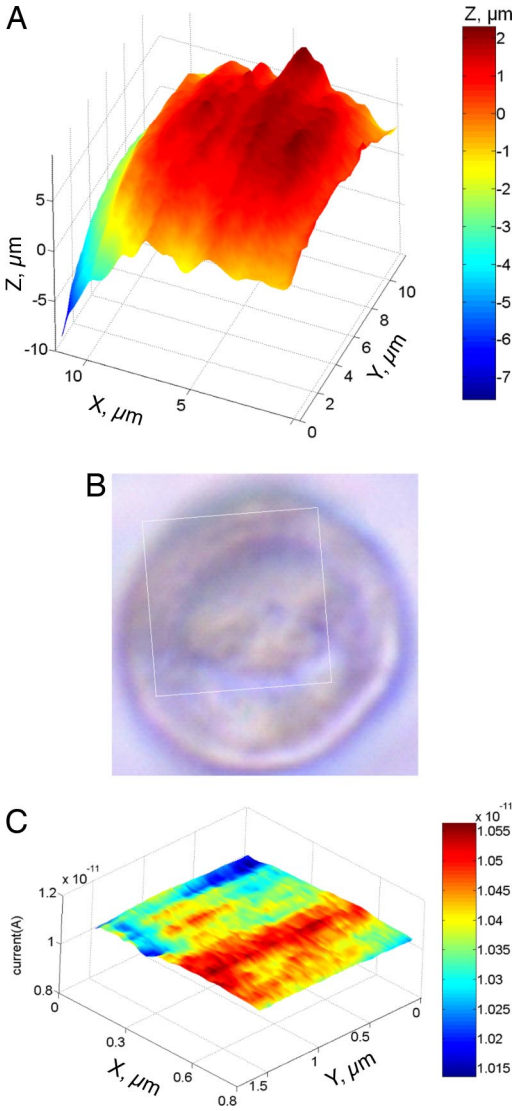

Fig. 6. Human breast epithelial (MCF-10A) cells imaged by the SECM. (*A*) 11.8 μm $\times$ 11.2 μm constant-current image of a cell obtained with a Pt tip (a = 123 nm, $r_g = 3a$). (*B*) Optical image of the same cell. The rectangular frame shows the area of the cell imaged in *A*. (*C*) Constant-height image of a 0.6 μm $\times$ 1.5 μm portion of cell surface obtained with a 47-nm tip. PBS contained 1 mM $Ru(NH_3)_6Cl_3$ as redox mediator.

slightly when the tip is moved inside the cell. Such variation may occur when additional membranes appear between the extracellular reference electrode and the tip as the latter enters a subcellular compartment (e.g., Golgi apparatus). To avoid this complication, one should extract $\Delta E_{1/2}$ from voltammograms obtained at the tip soon after it has penetrated the cell.

Measurements of transport rates across biomembranes are challenging even for model systems, for example, lipid bilayers (35). We have tried to evaluate the rate of the cross-membrane charge transport from extracellular SECM experiments by analysis of a model involving two additional steps. The P values measured in ref. 18 for the same mediator (menadione) and the same cell line (MCF-10A) were approximately one order of magnitude lower. Most likely, the results in ref. 18 were affected by a slow intracellular redox reaction. The intracellular SECM experiments are free from this problem. One should notice that a solution film always exists between the bottom of the cell and the surface to which it adheres. Although the film thickness of $\approx$10 nm (36) is too small to affect our measurements, a possible effect of the underlying gold surface on membrane permeability has yet to be investigated.

To our knowledge, the only reported nanoscale SECM images of biological samples are those of mouse monoclonal IgG, DNA, and other biomolecules obtained on a mica substrate in humid air (37). The main difficulty in feedback mode SECM imaging of living cells on the nanoscale is that the separation distance between the tip and the membrane has to be of the order of the tip radius. In the constant current mode (Fig. 6*A*), the constant distance between the tip surface and the cell is maintained, and the tip follows the cell contour (38). In this way, the entire cell or a major portion of it can be imaged with a high spatial resolution by using a tip radius much smaller that the cell dimensions. By using this approach, high-quality topographic images of neuron cells were obtained with a spatial resolution of $\approx$1 μm (14). Here, we used a small and very sharp tip with $r_g < 3a$ to increase the resolution to $\approx$200 nm.

The constant-height image (Fig. 6*C*) was obtained by scanning a 47-nm tip laterally above the cell in the x-y plane. If the tip radius is significantly smaller than the variations in height between different parts of a cell, either the higher parts get scratched in the process of imaging, or the lower parts are not imaged clearly. However, a small and relatively flat portion of the cell surface (e.g., 0.6 μm $\times$ 1.5 μm in Fig. 6*C*) can be imaged with the spatial resolution much higher than that in any reported SECM image of living cells.

A hydrophilic mediator used to obtain images in Fig. 6 could not permeate the cell membrane. Thus, both images represent only cell topography. In ref. 17, we mapped redox reactivity of mammalian cells with micrometer spatial resolution by using a hydrophobic mediator. A current-distance curve (Fig. 3) suggests that reactivity mapping can also be done at the nanoscale because some feedback from the cell could be seen when the tip approached its surface. The combination of SECM with fluorescence microscopy (39) should help one interpret such images and extract spatially resolved information on cellular redox reactivity.

Materials and Methods

Electrodes. A two-electrode setup was used for voltammetry and SECM experiments with a nanometer-sized Pt working electrode and a commercial Ag/AgCl reference. Evaporated Au films on glass were obtained as a gift from Alexander Vaskevich (Weizmann Institute of Science, Rehovot, Israel) and used as a conductive SECM substrate for CT rate measurements across the cell membrane. The preparation of polished, needle-like, disk-shaped nanotips was similar to the procedures described (40). In brief, 25-μm annealed Pt wires were pulled into borosilicate glass capillaries (1.0 mm o.d., 0.58 mm i.d.) under vacuum with the help of a P-2000 laser pipet puller (Sutter Instruments). The pulling program was modified by increasing the heat and velocity parameters to obtain a long and sharp tip with a thin glass sheath required for easier membrane penetration. The effective radius was evaluated from steady-state voltammetry and SECM (40).

Cell Culture. Midpassage MCF-10A cells, a human breast epithelial cell line, were cultured as described in ref. 17. Cells were plated at 5–20% confluence (2–8 $\times$ 10^3 cells per 60-mm plate) on the day before the experiment. For experiments requiring an underlying conductive surface, cells were cultured on a glass slide covered with an evaporated Au film, which was fixed in a culture dish. Before each experiment, adherent cells were rinsed with pH 7.4 PBS without calcium or magnesium (Cambrex), which was used as electrolyte in all electrochemical experiments.

Instrumentation and Procedures. All measurements were performed at ambient temperature in a plastic culture dish mounted on the horizontal stage of an Axiovert-100 inverted fluorescence microscope (Zeiss) that was set on an optical table. The cells were immersed in PBS containing the redox mediator. A home-built SECM instrument (40) was set on the same optical table as the microscope, so that the SECM tip could be positioned above the cell culture plate. Three types of experiments were performed: (i) i_T vs. d curves [approach

curves (31)] were obtained by positioning the tip above the cell and slowly moving it vertically down toward the cell surface, penetrating the cell, and continuing to move toward the underlying plastic or Au surface; (ii) topographic images of the cell were obtained by recording variations in tip current [constant-height mode (31)] or *z*-coordinate [constant-current mode (31)] while the probe was scanned laterally above the cell surface; and (iii) steady-state voltammograms were obtained by positioning the tip either above the cell or inside it and sweeping the tip potential.

In penetration experiments, when $Ru(NH_3)_6Cl_3$ was used as a redox mediator, solutions were deaerated. To prevent damage to the cells, oxygen was removed from the medium for a brief period that immediately preceded the actual measurements. The nearly complete removal of O_2 was evident from cyclic voltammetry (Fig. 2*B*, curve 2).

ACKNOWLEDGMENTS. This work was supported by National Science Foundation Grant CHE-0645958 and by the Professional Staff Congress City University of New York.

1. Finkel T (2003) Oxidant signals and oxidative stress. *Curr Opin Cell Biol* 15:247–254.
2. Houstis N, Rosen ED, Lander ES (2006) Reactive oxygen species have a causal role in multiple forms of insulin resistance. *Nature* 440:944–948.
3. Adler V, Yin Z, Tew KD, Ronai Z (1999) Role of redox potential and reactive oxygen species in stress signaling. *Oncogene* 18:6104–6111.
4. Wightman RM (2006) Probing cellular chemistry in biological systems with microelectrodes. *Science* 311:1570–1574.
5. Amatore C, *et al.* (2000) Analysis of individual biochemical events based on artificial synapses using ultramicroelectrodes: Cellular oxidative burst. *Faraday Discuss* 116:319–333.
6. Horrocks BR, Wittstock G (2001) in *Scanning Electrochemical Microscopy*, eds Bard AJ, Mirkin MV (Marcel Dekker, New York), pp 445–519.
7. Bard AJ, Li X, Zhan W (2006) Chemically imaging living cells by scanning electrochemical microscopy. *Biosens Bioelectron* 22:461–472.
8. Amemiya S, Guo J, Xiong H, Gross DA (2006) Biological applications of scanning electrochemical microscopy: Chemical imaging of single living cell and beyond. *Anal Bioanal Chem* 386:458–471.
9. Devadoss A, Burgess JD (2004) Steady-state detection of cholesterol contained in the plasma membrane of a single cell using lipid bilayer-modified microelectrodes incorporating cholesterol oxidase. *J Am Chem Soc* 126:10214–10215.
10. Mauzeroll J, Bard AJ (2004) Scanning electrochemical microscopy of menadione-glutathione conjugate export from yeast cells. *Proc Natl Acad Sci USA* 101:7862–7867.
11. Mauzeroll J, Bard AJ, Owhadian O, Monks TJ (2004) Menadione metabolism to thiodione in hepatoblastoma by scanning electrochemical microscopy. *Proc Natl Acad Sci USA* 101:17582–17587.
12. Amatore C, *et al.* (2006) Monitoring in real time with a microelectrode the release of reactive oxygen and nitrogen species by a single macrophage stimulated by its membrane mechanical depolarization. *ChemBioChem* 7:653–661.
13. Lu H, Gratzl M (1999) Monitoring drug efflux from sensitive and multidrug-resistant single cancer cells with microvoltammetry. *Anal Chem* 71:2821–2830.
14. Kurulugama RT, *et al.* (2005) Scanning electrochemical microscopy of model neurons: Constant distance imaging. *Anal Chem* 77:1111–1117.
15. Yasukawa T, Kaya T, Matsue T (2000) Characterization and imaging of single cells with scanning electrochemical microscopy. *Electroanalysis* 12:653–659.
16. Wittstock G, Burchardt M, Pust SE, Shen Y, Zhao C (2007) Scanning electrochemical microscopy for direct imaging of reaction rates. *Angew Chem Int Ed* 46:1584–1617.
17. Liu B, Rotenberg SA, Mirkin MV (2000) Scanning electrochemical microscopy of living cells: Different redox reactivities of human breast cells and metastatic breast cancer cells. *Proc Natl Acad Sci USA* 97:9855–9860.
18. Liu B, Rotenberg SA, Mirkin MV (2002) Scanning electrochemical microscopy of living cells. 4. Mechanistic Study of charge transfer reactions in human breast cells. *Anal Chem* 74:6340–6348.
19. Cans A-S, *et al.* (2003) Artificial cells: Unique insights into exocytosis using liposomes and lipid nanotubes. *Proc Natl Acad Sci USA* 100:400–404.
20. Zhan W, Bard AJ (2006) Scanning electrochemical microscopy. 56. Probing outside and inside single giant liposomes containing $Ru(bpy)_3^{2+}$. *Anal Chem* 78:726–733.
21. Ewing AG, Strein TG, Lau YY (1992) Analytical chemistry in microenvironments: single nerve cells. *Acc Chem Res* 25:440–447.
22. Arbault S, Pantano P, Jankowski JA, Vuillaume M, Amatore C (1995) Monitoring an oxidative stress mechanism at a single human fibroblast. *Anal Chem* 67:3382–3390.
23. Fasching RJ, Bai S-J, Fabian T, Prinz FB (2006) Nanoscale electrochemical probes for single cell analysis. *Microelectron Eng* 83:1638–1641.
24. Watkins JJ, *et al.* (2003) Zeptomole voltammetric detection and electron-transfer rate measurements using platinum electrodes of nanometer dimensions. *Anal Chem* 75:3962–3971.
25. Kraft ML, Weber PK, Longo ML, Hutcheon ID, Boxer SG (2006) Phase separation of lipid membranes analyzed with high-resolution secondary ion mass spectrometry. *Science* 313:1948–1951.
26. Korchev YE, Bashford CL, Milovanovic M, Vodyanoy I, Lab MJ (1997) Scanning ion conductance microscopy of living cells. *Biophys J* 73:653–658.
27. Betzig E, *et al.* (2006) Imaging Intracellular fluorescent proteins at nanometer resolution. *Science* 313:1642–1645.
28. Kwak J, Bard AJ (1989) Scanning electrochemical microscopy. Theory of the feedback mode. *Anal Chem* 61:1221–1227.
29. Swaminathan R, Hoang CP, Verkman AS (1997) Photobleaching recovery and anisotropy decay of green fluorescent protein GFP-S65T in solution and cells: Cytoplasmic viscosity probed by green fluorescent protein translational and rotational diffusion. *Biophys J* 72:1900–1907.
30. Wonderlin WF, Woodfork KA, Strobl JS (1995) Changes in membrane potential during the progression of MCF-7 human mammary tumor cells through the cell cycle. *J Cell Physiol* 165:177–185.
31. Bard AJ, Mirkin MV, eds (2001) *Scanning Electrochemical Microscopy* (Dekker, New York).
32. Miedema H, Assmann SM (1998) The calculation of intracellular ion concentrations and membrane potential from cell-attached and excised patch measurements. cytosolic k^+ concentration and membrane potential in vicia faba guard cells. *J Membr Biol* 166:101–110.
33. Schlue W-R, Kilb W, Gunzel D (1997) Ultramicroelectrodes for membrane research. *Electrochim Acta* 42:3197–3205.
34. Klymchenko AS, Stoeckel H, Takeda K, Mély Y (2006) Fluorescent probe based on intramolecular proton transfer for fast ratiometric measurement of cellular transmembrane potential. *J Phys Chem B* 110:13624–13632.
35. Amemiya S, Bard AJ (2000) Scanning electrochemical microscopy. 40. Voltammetric ion-selective micropipet electrodes for probing ion transfer at bilayer lipid membranes. *Anal Chem* 7:4940–4948.
36. Wegener J, Keese CR, Giaever I (2000) Electric cell–substrate impedance sensing (ECIS) as a noninvasive means to monitor the kinetics of cell spreading to artificial surfaces. *Exp Cell Res* 259:158–166.
37. Fan FRF, Bard AJ (1999) Imaging of biological macromolecules on mica in humid air by scanning electrochemical microscopy. *Proc Natl Acad Sci USA* 96:14222–14227.
38. Bauermann LP, Schuhmann W, Schulte A (2004) An advanced biological scanning electrochemical microscope (Bio-SECM) for studying individual living cells. *Phys Chem Chem Phys* 6:4003–4008.
39. Feng WJ, Rotenberg SA, Mirkin MV (2003) Scanning electrochemical microscopy of living cells. 5. Imaging of fields of normal and metastatic human breast cells. *Anal Chem* 75:4148–4154.
40. Sun P, Mirkin MV (2006) Kinetics of electron transfer reactions at nanoelectrodes. *Anal Chem* 78:6526–6534.